Monolithic MEMS Quadrupole Mass Spectrometers by Deep Silicon Etching

Martin Geear, Richard R. A. Syms, *Senior Member, IEEE*, Steven Wright, and Andrew S. Holmes, *Member, IEEE*

***Abstract*—A wafer-scale, batch fabrication process for constructing quadrupole mass spectrometers using microelectromechanical systems (MEMS) technology is described. The device is formed from two bonded silicon-on-insulator (BSOI) substrates, which are attached together to form a monolithic block. Deep etched features and springs formed in the outer silicon layers are used to locate cylindrical metal electrode rods, while similar features formed in the inner silicon layers are used to define integrated ion entrance and exit optics. The precision of the assembly is determined by lithography and deep etching, and by the mechanical definition of the bonded silicon layers. Mass filtering is demonstrated, with a mass range of $\approx$ 400 a.m.u. and a mass resolution of 1 a.m.u. at 219 a.m.u., using quadrupoles with rods of 500 μm diameter and 30 mm length, operating at 6 MHz RF frequency. [1447]**

***Index Terms*—Mass spectrometry, microelectromechanical systems (MEMS), quadrupole lens.**

I. Introduction

MINIATURE mass spectrometers are important as portable detectors of pollutants, drugs, explosives, and biological and chemical warfare agents [1], [2]. Thick film or microelectromechanical systems (MEMS) processes are increasingly being used to fabricate the complex electrode structures. Mass filters have been constructed as crossed-field [3]–[6], time-of-flight [7], [8], and cylindrical trap [9]–[13] types, and other MEMS components such as ion sources [14], [15] and detectors [16] are also being developed.

Here, we concentrate on the popular quadrupole mass spectrometer (QMS), which uses an electrostatic lens as a mass filter [17]. Quadrupoles consist of four cylindrical electrodes, mounted parallel and with their spacing at a well-defined ratio to their diameter. Ions are injected into a pupil between the electrodes, and travel parallel to them under the influence of a time-varying hyperbolic electrostatic field that contains both a direct current (dc) and an alternating current (ac) component. The ac frequency is fixed, as (in the simplest operational mode) is the ratio of the dc and ac voltages. Studies of ion dynamics in such a field have shown that only ions near a particular mass-to-charge ratio will transit without discharging on a rod. If the voltage amplitudes are ramped, the time variation of the output ion flux is a mass spectrum [18], [19].

Resolution is determined by two main factors: the number of cycles of ac field experienced by each ion, and the accuracy with which the field is created. The ions are therefore injected with a small axial velocity, and a radio frequency (RF) drive is used. Highly accurate methods of construction must be used to create the desired hyperbolic field. However, it is increasingly difficult to obtain suitable precision as sizes are reduced. The mass range is limited by the maximum voltage, and the sensitivity by the ion flux (which also clearly reduces as the size of the pupil is decreased) [18], [19].

Several miniature QMS systems have been constructed. For example, two instruments based on arrays of electrostatic quadrupoles have been developed [20], [21]. Smaller quadrupole arrays have been fabricated by exposing a photoresist to synchrotron radiation and filling the resulting mould with nickel by electroplating [22]. The lens assembly is a planar element, and configured into a stacked structure in the complete mass spectrometer.

A rather different MEMS quadrupole was developed in the mid-1990s by Imperial College and Liverpool University. The device consists of four cylindrical electrodes mounted in pairs on two oxidised, silicon substrates that are held apart by two cylindrical spacers [23]–[25]. V-shaped grooves formed by anisotropic etching locate the electrodes and the spacers. The electrodes are metal-coated glass rods soldered to metal films deposited in the grooves. A QMS with electrodes of square cross-section has also been constructed by others [26].

Mass filtering with a range just over 100 atomic mass units (a.m.u.) has been demonstrated using devices with electrodes of 500 μm diameter and 30 mm length [25]. However, the approach has disadvantages. The rods require lengthy preparation, and rod bonding is also a time consuming manual operation. Additional fixtures are needed to hold the assembly together, and there is no axial alignment of the substrates. There are also serious performance limitations. Most importantly, strong capacitive coupling across the oxide layer at the RF drive frequency gives rise to resistive heating in the silicon substrate. At higher voltages this tends to melt the solder, causing the rods to detach. The large mismatch in temperature coefficient of expansion (TCE) between the glass rods and the silicon can also be an issue. These effects limit the maximum drive voltage (and thus the mass range) that can be achieved.

In addition, the construction forms only a mass filter, and at the very least an ion source and a detector must be added to form a complete QMS. Some attempt has been made to integrate input coupling optics [27]; however, only one-dimensional focussing

Manuscript received October 15, 2004; revised January 5, 2005. This research was funded by the Home Office Police Scientific Development Branch under PSDB Contract 3611. The paper was additionally funded by Dstl. Subject Editor H. Fujita.

M. Geear and S. Wright are with the Microsaic Systems Ltd., Woking, Surrey GU21 5BX, U.K.

R. R. A. Syms and A. S. Holmes are with the Optical and Semiconductor Devices Group, Electrical and Electronic Engineering Department, Imperial College London, London SW7 2BT, U.K. (e-mail: r.syms@ic.ac.uk).

Digital Object Identifier 10.1109/JMEMS.2005.851799

1057-7157/$20.00 © 2005 IEEE

has been achieved, and it is difficult to see how other important features (a closed source cage, or gas inlet channels) may be integrated. The design therefore has major evolutionary limits.

In this paper, we demonstrate an entirely new approach to MEMS quadrupole mass spectrometers, which overcomes these limitations. Fabrication is based on deep reactive ion etching and stacking of bonded silicon-on-insulator (BSOI) substrates. This approach allows significant improvements to the mechanical, thermal and electrical characteristics, which in turn yield increased mass range and resolution. The result is a rugged, monolithic component, which contains fully integrated input and output optics. Most importantly, the system also has the potential for future cointegration of many other elements. A brief summary of the principle of quadrupole mass filtering is given in Section II. The overall design is presented in Section III, and fabrication of prototype devices is described in Section IV. Mass filtering is described in Section V, and conclusions are presented in Section VI.

II. The Quadrupole Mass Filter

We begin with a short explanation of the quadrupole mass filter [18]. An ideal quadrupole consists of four parallel electrodes with hyperbolic cross-sections, which carry potentials $\pm\phi_0/2$ as shown in Fig. 1(a). These electrodes establish the two-dimensional (2-D) potential field

$$\phi(x,y)=\frac{\phi_0(x^2-y^2)}{2r_0^2}. \quad (1)$$

Here r_0 is the radius of the circle touching the equipotentials $\phi = \pm\phi_0/2$. Because of the difficulty of machining hyperbolic electrodes, cylindrical rods are generally used. There is some debate as to the most suitable electrode radius r_e. The ratio $r_e = 1.148\ r_0$ is a popular choice, and gives an excellent approximation to (1). For 500 μm diameter electrodes (for example), we then have $r_0 \approx 217.8\ \mu\text{m}$. However, nearby grounded structures alter the optimum, and a modified value of r_e/r_0 has been found for earlier MEMS quadrupoles [24].

The electrostatic field will exert forces in both the x- and y-directions on an ion moving in the z-direction. The equations of motion are

$$\frac{md^2x}{dt^2}=\frac{-e\partial\phi}{\partial x}=\frac{-e\phi_0 x}{r_0^2}$$
$$\frac{md^2y}{dt^2}=\frac{-e\partial\phi}{\partial y}=\frac{+e\phi_0 y}{r_0^2} \quad (2)$$

where e and m are the charge and mass of the ion. When the time variation of the potential is $\phi_0(t)=U-V\cos[\omega(t-t_0)]$, where $\omega=2\pi f$ is an angular frequency, ωt_0 is the starting phase and U and V are constant potentials, the equations of motion reduce to

$$\frac{d^2(x,y)}{dt^2}\pm\left(\frac{e}{mr_0^2}\right)\{U-V\cos[\omega(t-t_0)]\}(x,y)=0. \quad (3)$$

Using the substitutions $t=2\zeta/\omega$, $t_0=2\zeta_0/\omega$, $a=4eU/\left(m\omega^2r_0^2\right)$ and $q=2eV/\left(m\omega^2r_0^2\right)$, (3) can be reduced to the Matthieu-like equations

$$\frac{d^2u}{d\zeta^2}+\{a_u-2q_u\cos[2(\zeta-\zeta_0)]\}u=0 \quad (4)$$

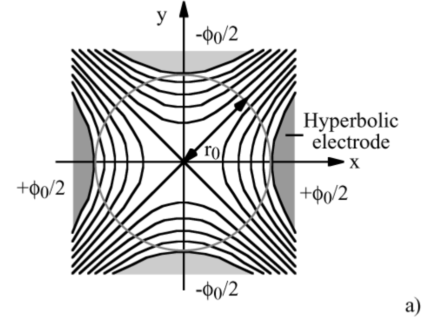

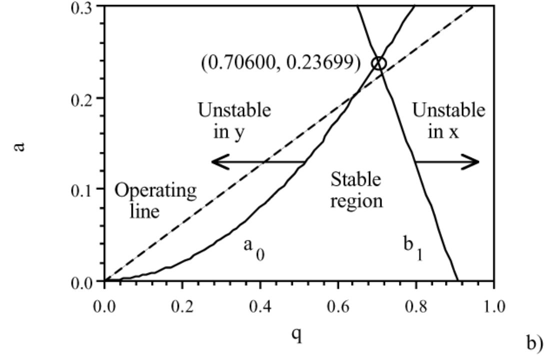

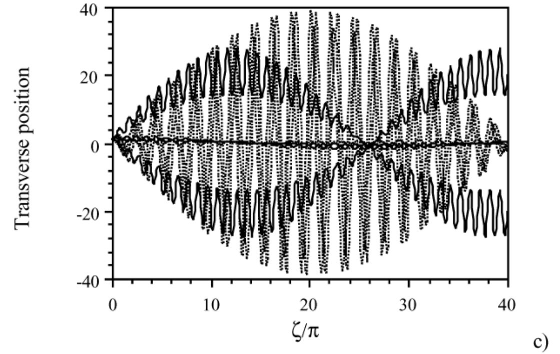

Fig. 1. (a) Hyperbolic electrostatic field; (b) lower stability diagram on the $q-a$ plane; (c) ion trajectories in x- and y-directions for $a/2q=0.167$ and $q=0.706$.

where u is x or y, and $a=a_x=-a_y$ and $q=q_x=-q_y$. The nature of the trajectory depends almost entirely on a and q, varying little with the initial conditions ζ_0, $u(0)$ and $u'(0)$. There are a several regions on the $q-a$ plane that give rise to stable solutions. The lower stability region is an approximately triangular region, bounded by the lines [18]

$$a_0(q)=\frac{q^2}{2}-\frac{7q^4}{128}+\frac{29q^6}{2304}\cdots$$
$$b_1(q)=1-q-\frac{q^2}{8}+\frac{q^2}{64}-\frac{q^4}{1536}-\frac{11q^5}{36\,864}\cdots. \quad (5)$$

These loci are shown in Fig. 1(b). The line a_0 defines the limit for trajectories that are stable in the y-direction, while b_1 is the similar limit for trajectories in the x-direction. Between the two, trajectories are stable in both directions. The apex of the stable region lies at $a=0.236\,99$, $q=0.706\,00$, so that $a/2q=U/V=0.167\,839\,9$.

For example, Fig. 1(c) shows x-trajectories (dotted lines) and y-trajectories (full lines) found from (4), assuming initial conditions of $x(0)=1$, $x'(0)=0$, $y(0)=1$, $y'(0)=1$ and four different starting phases, for $a/2q=0.167$ and $q=0.706$ (just

below the apex). In all cases, the trajectories are bounded. For lower q (i.e., higher mass) the trajectories are unstable in the y-direction, and for higher q (lower mass) they are unstable in the x-direction. Normally, U and V are ramped together, following the operating line passing just below the apex of the lower stability region of different masses. Stable trajectories are only obtained for a narrow mass range, so that the device acts as a tuneable mass filter.

The use of a scan line passing close to the stability tip requires potentials $U \approx 0.236\,99\left(m\omega^2 r_0^2/4e\right)$ and $V \approx 0.706\,00\left(m\omega^2 r_0^2/4e\right)$. An attractive feature of miniaturization is that U and V scale with r_0^2, so that decreasing the linear dimension of an instrument by a factor of (say) 10 will reduce both potentials 100-fold. For a quadrupole with 500 μm diameter electrodes, we obtain $U = 0.041\,69$ m Volts, where m is measured in a.m.u. For a mass range of (say) 400 a.m.u., we therefore require $U_{\max} \approx 16.67$ Volts, and similarly $V_{\max} \approx 99.35$ Volts. These values correspond to peak dc and ac voltages at the rods of ≈ 8.3 and 50 volts, respectively, which are conveniently developed with simple electronics.

Based on experimental evidence (see, e.g., [18]), it has been shown that the best attainable fractional mass resolution varies as $m/\Delta m \approx n^2/20$, where n is the number of cycles of the RF field experienced by an ion in transit. Ions are normally injected with a constant axial energy V_z, and hence a mass-dependent velocity $v = \sqrt{(2eV_z/m)}$. The number of cycles is therefore $n \approx fL/v$, where L is the quadrupole length, so the uncertainty in mass is

$$\Delta m \approx \frac{40eV}{(f^2L^2)}. \tag{6}$$

If Δm is in a.m.u., this can be written as $\Delta m \approx 3.854 \times 10^9\ V_z/(f^2L^2)$. A quadrupole with electrodes with $L = 30$ mm, operating at $f = 6$ MHz, would therefore have a resolution of 0.03 a.m.u. when $V_z = 10$ V. However, this resolution is often not reached; throughput drops significantly as the resolution rises, and there is a direct trade-off between sensitivity and resolution. Since Δm is theoretically independent of m, $m/\Delta m$ increases with mass. However, offset operating lines or operating curves are often required to achieve this result in practise.

III. Monolithic MEMS Quadrupole Mass Spectrometers

In developing a MEMS quadrupole mass spectrometer, the challenge is to devise methods of electrode rod mounting that are compatible with the incorporation of other features needed in the complete system. In [24], the rods were mounted in V-shaped grooves etched on the *inner* surfaces of two separated substrates. Here, we present an entirely new mounting that locates the rods in the *outer* layers of a stacked wafer assembly.

The rods are precision-machined metal cylinders, which are held in vertically etched slots by silicon springs, following methods used to locate fibers in optical MEMS [28]. This approach simplifies assembly, avoids the need for bonding and reduces the likelihood of detachment. The slots and springs are formed in BSOI substrates [29], [30], using deep-reactive ion etching (DRIE) methods that are now highly developed for MEMS [31]. The precision of the structure is therefore determined by lithography and deep etching, and by the original definition of the bonded silicon layer.

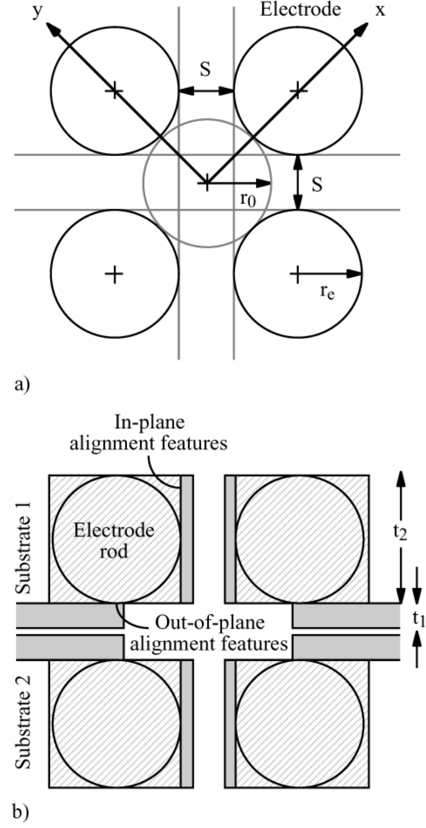

Fig. 2. (a) Principle of electrode rod alignment and (b) stacked substrate assembly in a monolithic MEMS quadrupole mass spectrometer.

The quadrupole geometry is achieved using two substrates, which are bonded together following methods developed for power MEMS devices [32]. The use of a monolithic block increases rigidity and reliability, and avoids the need for additional components to align the structure or hold it together. Electrical isolation is provided by thick layer of high quality SiO_2, minimizing leakage and maximizing the voltage that can be applied. The majority of the silicon around the rods is removed, minimizing capacitance coupling and maximizing the usable frequency. The overall fabrication scheme is extremely flexible, and many additional features such as ion coupling optics may easily be incorporated.

Fig. 2(a) shows the principle. The electrode rods are positioned by two sets of orthogonal, planar interior features. Each set involves two planes a distance S apart, where S is given by

$$S = r_e\left\{(\sqrt{2} - 2) + \sqrt{2}\left(\frac{r_0}{r_e}\right)\right\}. \tag{7}$$

These planes may be provided in a stacked assembly as shown in Fig. 2(b). Two BSOI substrates are used. Each contains a device layer of thickness $t_1 = S/2$, and a substrate of thickness $t_2 \approx 2r_e$. The two layers are separated using a thin insulating layer. Out-of-plane alignment features for the electrode rods are formed in the first layer, while in-plane features are formed in the second. For an electrode rod radius of (say) $r_e = 250\ \mu$m,

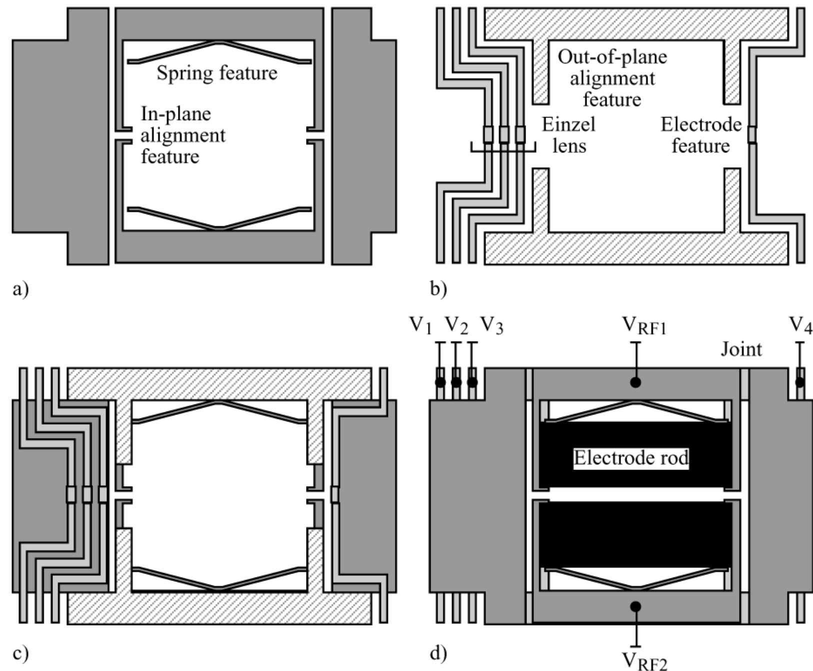

Fig. 3. Layout of (a) outer and (b) inner etched patterns; (c) overlay of the two patterns and (d) location of the electrode rods in a monolithic MEMS quadrupole mass spectrometer.

the required thickness values are $t_1 \approx 81\ \mu\mathrm{m}$ and $t_2 \approx 500\ \mu\mathrm{m}$. The first value may be achieved simply by using an a suitable device layer thickness. The substrates are stacked back-to-back, so that a total out-of-plane separation S is obtained between the rods. A small gap is used for electrical isolation between the rods on each substrate.

Two double-side-polished BSOI substrates are required, which may be formed on the same wafer. Each is patterned by DRIE with an outer pattern on the substrate side, and an inner pattern on the device layer. There is considerable flexibility in the features that may be incorporated. Fig. 3 shows an example. It should be noted that this figure is distorted for ease of representation; the electrode rods are considerably longer in a real device.

The outer pattern is shown in Fig. 3(a), and consists of a set of locating features for two of the four electrode rods. Leaf springs are used to retain the rods, contacting the rods at their extremities to avoid bending. The rods can slide slightly in the axial direction, relieving stress caused by differential thermal expansion. The springs are placed outside the quadrupole, so that the important axial region is clear of any structure likely to perturb the electrostatic field, except at the input and output. The inner pattern is shown in Fig. 3(b) and contains further electrostatic optics. At the left-hand end, there is a set of three electrodes arranged as an einzel lens, a common input coupling element. At the right-hand end, there is a second set of electrodes for output coupling. Multi-layer etching is used to limit the depth of some features, so that a thin silicon bridge is left linking the upper and lower parts of the einzel lens to form a pupil. The shaded out-of-plane alignment features are also thinned slightly, to avoid electrical contact with their counterparts on the second substrate. Each set of features comprises half the overall structure, so that the complete pupil created by the bonding operation. There are clearly restrictions on the pupil size and shape, which must normally be rectangular. The resulting components are therefore astigmatic. However, there is considerable scope to shape the electrodes in plane, for example to improve coupling, and many other buried features may be incorporated.

Fig. 3(c) shows the relationship of the two patterns. Some features in the outer pattern are used to ensure mechanical continuity between sections; other features such as scarf joints may be used to ensure electrical isolation. The outer layer pattern is cut away to allow single-sided access to all the buried electrodes. Fig. 3(d) shows the eventual location of the cylindrical electrode rods within the outer layer. The locating springs hold the two rods symmetrically on either side of an optical axis defined by the entrance and exit pupils. The springs also make electrical contact to the electrode rods. The oxide interlayer is partially removed, so that there is structural continuity between the layers only in the regions where the patterns overlap. Metallization is used to allow contact to each electrode and spring.

Assembly may be carried out on a die-by-die or wafer-scale basis. Two etched substrates are aligned and bonded to leave a silicon-oxide-silicon-oxide-silicon multilayer stack, as previously shown in Fig. 2(b). At this stage, each device is a single rigid, monolithic block. Each device is then attached to a submount, and wire-bond connections are made to the contact metallization. Connections to otherwise buried features are made by etched via holes. Finally, electrode rods are inserted into the block.

IV. Fabrication of Prototypes

We have developed a four-mask process for wafer scale fabrication of quadrupoles as described in the previous section, with electrode rods of 500 $\mu\mathrm{m}$ diameter and 30 mm length. Using wafers of 100 mm diameter, each wafer yields sufficient dies

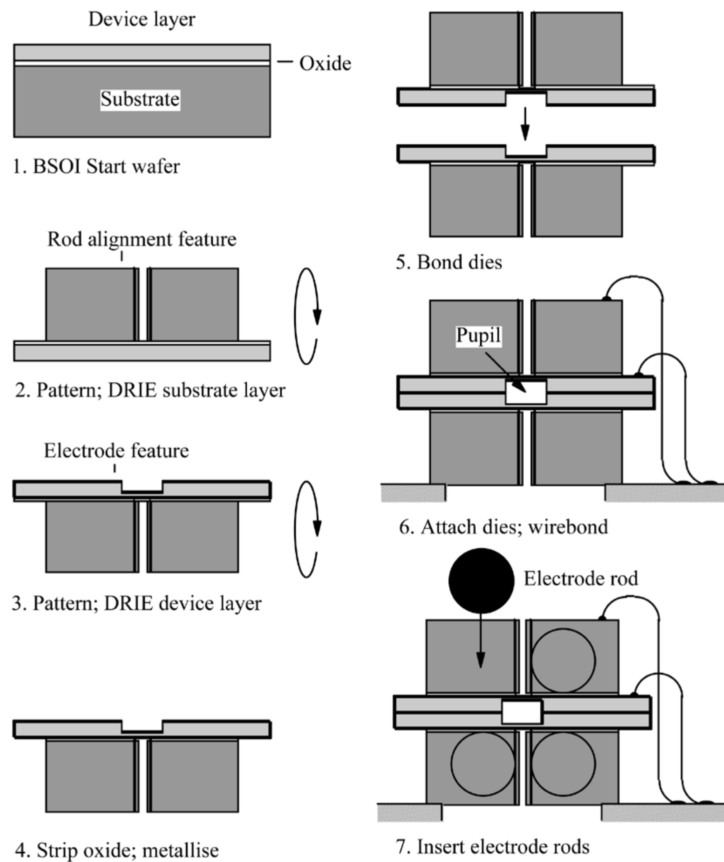

Fig. 4. Process flow for device fabrication.

for construction of 10 mass spectrometers. The process is summarized in Fig. 4. The starting point is a D/S polished, (100) oriented BSOI wafer with a device layer thickness of $\approx 80\ \mu m$ and an oxide thickness of 2 μm (Step 1). Substrates between 450 μm and 350 μm thick have been used successfully. The in-plane positions of the electrode rods are defined by tangent contact with features etched in this layer.

A hard mask layer consisting of a thick layer of Shipley AZ9260 photoresist is first deposited on the substrate side, and patterned with the outer layer features (Mask #1). This pattern is transferred through the substrate to the oxide interlayer (Step 2), using a Surface Technology Systems Single-chamber Multiplex inductively coupled plasma (ICP) etcher, operating a variant of the cyclic etch-passivate process based on SF_6 and C_4F_8 developed by Robert Bosch GmbH [31], [33]. The etch selectivity is $\approx 100 : 1$. The hard mask is then removed using a commercial wet resist stripper followed by oxygen plasma.

Excellent verticality is achieved during substrate patterning, and the etched features are accurate and robust enough to locate the electrode rods. For example, Fig. 5(a) is a scanning electron microscope (SEM) photograph of an outer layer pattern formed in a bare Si substrate, showing parallel mounting of electrode rods by the two leaf springs. Fig. 5(b) shows a detail of the electrode rod alignment fixture; comparatively small features can be used to hold the rod ends in place without fracturing the silicon.

The device layer side is then patterned using a set of masks defining the inner layer features. Front-to-back alignment is carried out using a Quintel IR-4000 mask aligner with through-wafer infrared illumination. First, the device layer is modified in areas that must be isolated from corresponding features on the second substrate. This step involves a relatively coarse pattern (Mask #2). The device layer electrodes are then defined using two more complex patterns (Masks #3 and #4). Two hard mask layers consisting of photoresist on thermal oxide are used, arranged in a stacked configuration to allow multi-level etching [34]. The patterns are again transferred through the silicon to the oxide interlayer by ICP etching (Step 3). Because the wafer contains now many completely open areas, proprietary techniques are used to ensure structural integrity. The hard masks are again stripped.

The oxide interlayer is then partly removed using concentrated (48%) HF. Careful layout is used to avoid stress-induced distortion of the dies in this step [35]. The wafer is metal-coated on both sides by RF sputtering with Cr and Au (Step 4). The dies are separated, using a simple snap-out procedure, and transferred in pairs to a die-bonding rig where they are attached together (Step 5). Alignment is obtained using precision etched features. Several bonding agents have been used successfully, including conductive epoxies and eutectic solders; however, direct wafer bonding could offer a more reliable alternative.

Registration of the patterns on each side of the wafer is routinely achieved to an accuracy of $\pm 2\ \mu m$. Dies are bonded together with a similar accuracy. For example, Fig. 5(c) shows an axial view of the input lens in a stacked wafer assembly. The two substrates lie at the top and bottom of the photo. In the centre,

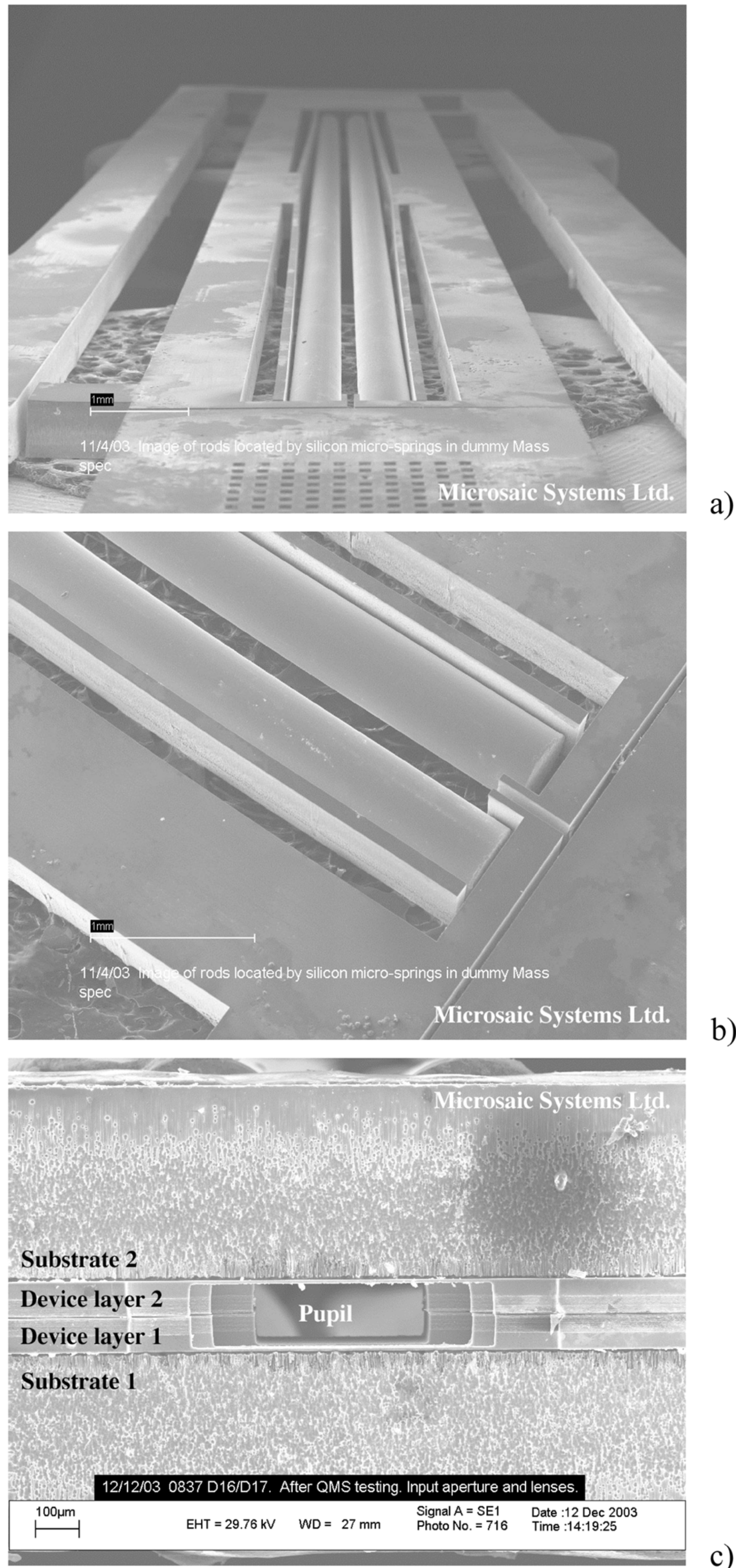

Fig. 5. SEM photographs, showing (a) spring mounting of electrode rods; (b) electrode rod alignment fixture; (c) input einzel lens in a stacked wafer assembly.

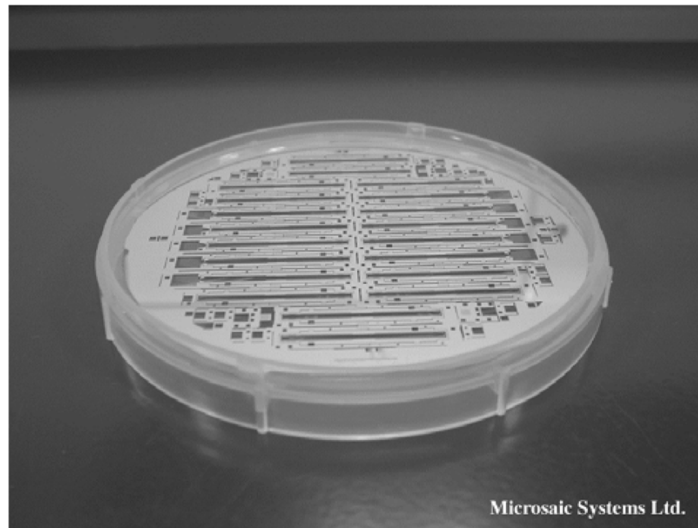

a)

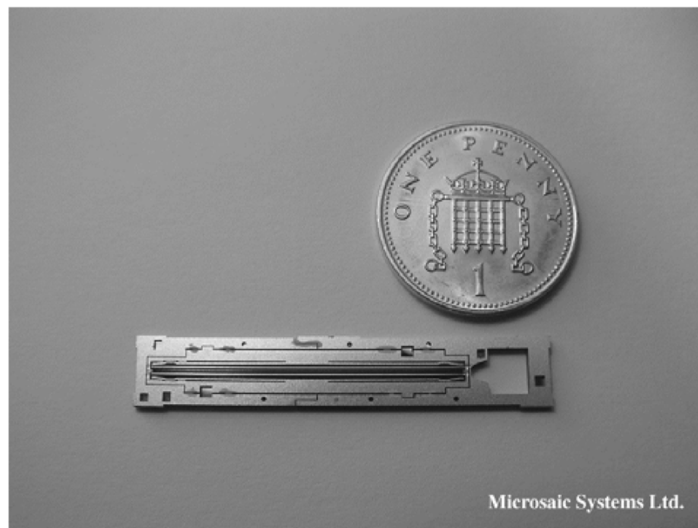

b)

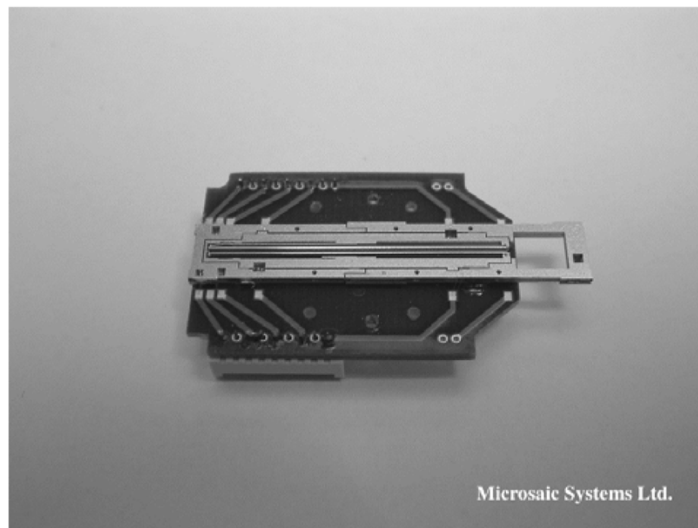

c)

Fig. 6. Optical photographs, showing (a) completed dies before snap out from wafer, (b) assembled mass spectrometer chip, and (c) chip attached to a PCB on a submount.

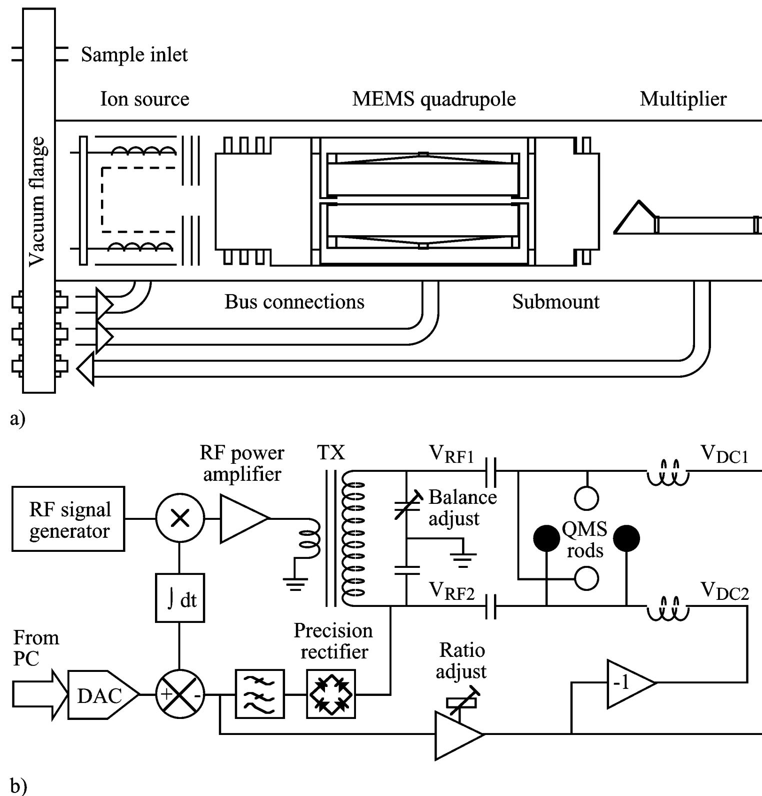

Fig. 7. (a) Experimental layout for device testing and (b) schematic of quadrupole drive electronics.

the device layers form the rectangular entrance pupil. Three concentric apertures forming the einzel lens may be seen; these are nested to improve coupling to the ion source. The electrode rods are just visible behind the entrance optics.

Completed dies are then attached to a PCB, and wire-bonds are taken to the electrical contacts (Step 6). In the example shown here, dc voltages V_1, V_2 and V_3 are applied to the input einzel lens electrodes and V_4 to the exit electrodes. Voltages $V_{\rm RF1}$ and $V_{\rm RF2}$ containing both a dc and an ac component are applied to the cylindrical electrodes. Finally, nonmagnetic stainless steel electrodes are inserted into the sprung alignment locations (Step 7).

Fig. 6(a) is an optical photograph showing completed dies before snap-out from the wafer, which clearly contains many open areas. Despite this, high die yields $(> 80\%)$ have been achieved without the need for special wafer handling equipment. Fig. 6(b) shows an assembled mass spectrometer chip with electrode rods inserted. The open area at the right-hand side is the detector location. Fig. 6(c) shows a chip mounted on a PCB, which is in turn attached to a sub-mount for vacuum testing. Here, tracking is used to route the various drive voltages from multi-way connectors.

V. Experimental Evaluation

Devices have been evaluated using a conventional thermal impact ionization source and a multiplying detector in a turbo-pumped vacuum system capable of reaching a base pressure of 10^{-8} mbar. The mass range and mass resolution obtained even in preliminary experiments have both been considerably improved compared with earlier MEMS quadrupoles [25].

Prototypes were mounted on a vacuum flange with an ion source and detector for testing as shown in Fig. 7(a). The ion source was a VG Anavac 1-3-1 type, located 0.5 mm from the quadrupole input. Experiments were performed at a pressure 2×10^{-5} mbar, with an electron energy of 60 eV, an emission current of 5 mA, and an axial ion energy of 10 eV. The einzel outer electrode voltages were $V_1 = V_3 = 0$ V, the focus voltage V_2 was variable, and the exit electrode voltage was $V_4 = 0$ V. The detector was a Detech 2120 channeltron from Detector Technology Inc. operated at 1.7 kV. The multiplier was arranged parallel to the quadrupole axis but offset to avoid a line of sight for photons and neutrals. Signals were detected in analogue mode, using a Keithley 6485 picoammeter for signal conditioning.

Assembled quadrupoles represent an approximately pure capacitative load of ≈ 68 pF. Resonant quadrupole drive electronics were constructed for operation in the range 2–10 MHz, with a frequency of 6.1 MHz being used in this work. Fig. 7(b) shows a block diagram of the quadrupole controller. The anti-phase RF signals $V_{\rm RF1}$ and $V_{\rm RF2}$ were derived from a signal generator using a RF power amplifier with a transformer-coupled output. Additional variable capacitive loading was used to achieve the desired resonant frequency, and ensure precise matching of the RF amplitudes on the two pairs of rods. A dc voltage proportional to the RF output was derived using a precision rectifier/low-pass filter combination. This voltage was used for closed-loop control of the RF output, and also to generate the dc quadrupole signals $V_{\rm dc1}$ and $V_{\rm dc2}$. The RF and dc signals were combined at the quadrupole using a standard bias tee arrangement. Mass scanning was controlled by a single

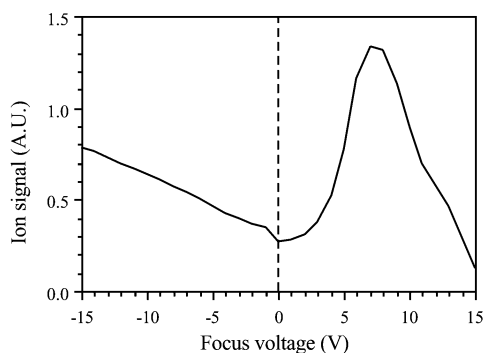

Fig. 8. Variation of ion signal with focus voltage V_2, at 69 a.m.u.

RF set-point voltage, which was generated by a PC running LabView™. The quadrupole was operated at a programmed dc/RF ratio so that the scan line cut the lower stability region close to its apex. The ratio was set by means of a variable gain amplifier in the dc path.

Initial tests were performed with $C_{12}F_{27}N$ (perfluorotributylamine, or PFTBA; molecular weight 671.09), a compound often used for instrument calibration [2]. The sample was introduced as follows. The liquid PFTBA was contained in a stainless steel phial connected to a leak valve. The phial was immersed in liquid N_2 to freeze the sample, and the air above was pumped away. The sample was then thawed and admitted to the vacuum chamber. Ion throughput was first optimized by adjusting the voltage V_2 applied to the central or focus electrode of the einzel lens. Fig. 8 shows the variation of the detected signal with V_2, obtained at 69 a.m.u., when the detected signal was the strongest. There is a clear peak at around $+7.0$ V, when the lens is operating in decelerating mode. The focus voltage was fixed at this value to obtain full spectra.

Fig. 9(a) shows background-subtracted mass spectra for PFTBA. The magnified inset spectrum was recorded at slightly lower resolution to enhance the higher mass peaks. Fig. 9(b) shows a reference spectrum obtained from a national standards laboratory [36]. Clear assignment of the individual mass peaks to known molecular fragments of PFTBA may be carried out to over 300 a.m.u. The resolution (FWHM) is 0.8 for the mass peak at 69 a.m.u. (CF_3) and 2.1 for the peak at 219 a.m.u. (C_4F_9) Higher peaks may be seen at 264 a.m.u. $(C_5F_{10}N)$ and also at 314 a.m.u. $(C_6F_{12}N)$. Smaller and less clearly identifiable peaks can be seen up to 396 a.m.u. However, the peak at 348 a.m.u is not attributable to PFTBA, and is assumed to be from a contaminant. Also present in Fig. 9(a) are peaks due to the usual residual gases H_2, H_2O, N_2/CO and O_2, which have masses of 2, 18, 28, and 32 a.m.u., respectively.

Fig. 10(a) and (b) show enhanced spectra for the mass peaks near 69 a.m.u. and 219 a.m.u., respectively, obtained by adjusting the scan parameters separately to give optimum results for each. In each case, the peak shape is slightly asymmetric. The resolutions achieved are 0.6 and 1.0, respectively; the latter figure corresponds to a fractional resolution $m/\Delta m$ of over 200.

These results represent an approximate four-fold increase in mass range and two-fold increase in resolution, compared with earlier MEMS quadrupoles [25]. Devices have operated successfully for many weeks without signs of thermal damage,

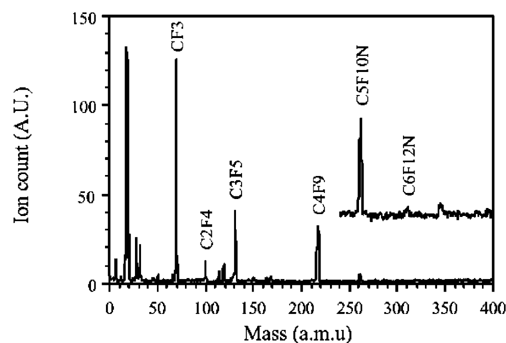

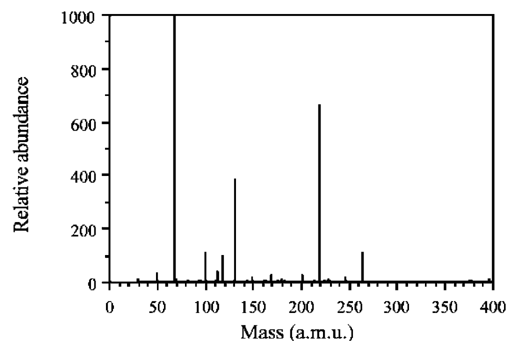

Fig. 9. (a) Mass spectrum for PFTBA and (b) reference spectrum (data courtesy NIST).

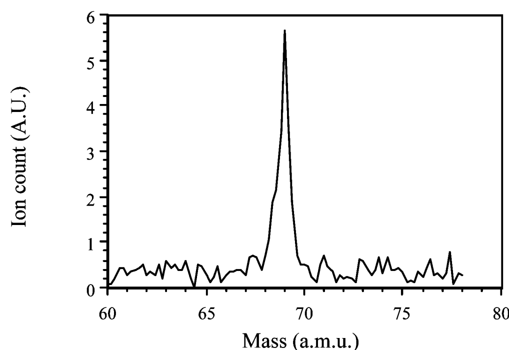

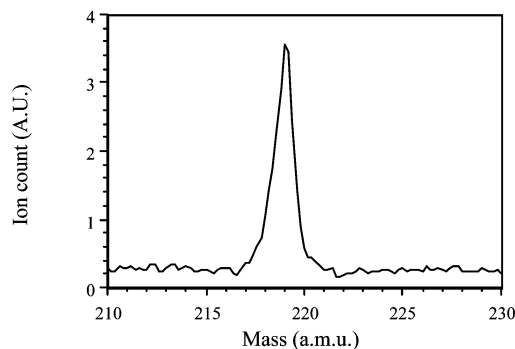

Fig. 10. Detail of mass peaks in PFTBA spectrum at (a) 69 a.m.u. and (b) 219 a.m.u.

and electrode rods have been removed and replaced for inspection and cleaning. This performance confirms the validity of the new approach to MEMS quadrupole design. Currently, we

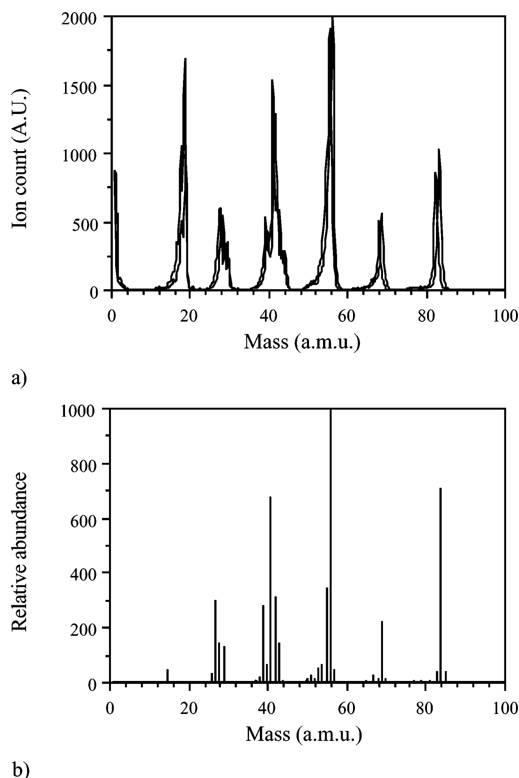

Fig. 11. (a) Superimposed mass spectra for cyclohexane, obtained from a different mass filter and (b) reference spectrum (data courtesy NIST).

are unable to measure overall fabrication accuracy to a suitable level by direct metrology. However, its value may be inferred from performance by comparison with experimental data obtained from conventional devices. Previously, it has been found that the maximum resolution is proportional to constructional error raised to the power of -1.3 [18]. Here, "constructional error" is defined as $(2\varepsilon + \varepsilon')/D$, where ε' is the general manufacturing tolerance, ε' is any deliberately introduced error and $D = 2r_e$. Experimental confirmation was obtained by deliberately altering the position of one rod with a micrometer, and it was found that a maximum resolution of 100 requires a constructional error below 1%. Since the results above suggest that this performance has already been exceeded using a MEMS quadrupole with $D = 500\ \mu\text{m}$, we may assume an overall accuracy of a few microns.

To demonstrate repeatability, Fig. 11(a) shows two separate mass spectra for cyclohexane, C_6H_{12}. The sample was introduced by the freeze-pump-thaw method, and measurements were obtained at a pressure of 3×10^{-6} mbar. The two spectra were obtained before and after some adjustments to the source conditions (to 70 eV electron energy), using a different MEMS mass filter to the device that generated the data of Figs. 8–10. The two spectra are essentially similar, with a maximum of less than 1 a.m.u. difference in the peak positions, and correspond well to the reference spectrum shown in Fig. 11(b) [36]. The additional peaks at low mass values again correspond to background O, OH, H_2O, and so on, and the regular appearance of sets of peaks separated by 14 a.m.u. is caused by the loss of CH_2 groups from basic units.

VI. Conclusion

We have demonstrated a new wafer-scale, batch fabrication process for constructing MEMS quadrupole mass spectrometers. The process offers considerable improvement in mechanical, thermal and electrical performance compared with earlier MEMS quadrupoles, which in turn has led to an increase in both mass range and resolution.

The quadrupole geometry is achieved using two BSOI substrates, which are bonded together to form a monolithic block. Deep etched features and springs formed in the outer silicon layers are used to locate cylindrical metallic electrode rods, while similar features formed in the inner silicon layers are used to define ion entrance and exit optics. The precision of the assembly is determined by a combination of lithography and DRIE, and by the mechanical definition of the bonded silicon layers. Both may be extremely high. The geometry offers considerable scope for cointegration of other features needed in complete mass spectrometer systems, such as gas or fluid inlet channels.

Preliminary experiments have been carried out to demonstrate mass filtering, using a conventional ion source and multiplying detector. A mass range of ≈ 400 a.m.u., and a mass resolution of $m/\Delta m \approx 219$ at $m = 219$ a.m.u., have been achieved using quadrupoles constructed with 500 μm diameter, 30 mm long stainless steel electrode rods and operated at 6 MHz. Attention is now being given to improvements in sensitivity and resolution and to the cointegration of other features.

Acknowledgment

The authors are extremely grateful for the support and encouragement of A. Finlay and Dr. E. Yeatman. The authors would like to acknowledge the help given by Prof. D. Lacey and Dr. S. Haque. The authors would also like to thank Dr. D. Groves for the support.

References

[1] C. M. Henry, "The incredible shrinking mass spectrometer," *Anal. Chem.*, vol. 71, pp. 264A–268A, 1999.
[2] E. R. Badman and R. G. Cooks, "Special feature: Perspective—Miniature mass analyzers," *J. Mass. Spect.*, vol. 35, pp. 659–671, 2000.
[3] F. C. Sittler, "Micromachined Mass Spectrometer," US 5 401 963, 1995.
[4] C. B. Freidhoff and R. M. Young, "Miniaturized Mass Filter," U.S. 5 536 939, Jul. 16, 1996.
[5] C. B. Freidhoff, "Mass spectrograph on a chip," in *Proc. 1997 IEEE Aerospace Conference*, vol. 3, Aspen, Colorado, Feb. 8, 1997, pp. 32–32.
[6] J. A. Diaz, C. F. Giese, and W. R. Gentry, "Sub-miniature $E \times B$ sector-field mass spectrometer," *J. Amer. Soc. Mass Spect.*, vol. 12, pp. 619–632, 2001.
[7] H. J. Yoon, J. H. Kim, T. G. Park, S. S. Yang, and K. W. Jung, "The test of hot emission for the micro mass spectrometer," *Proc. SPIE*, vol. 4408, pp. 360–367, 2001.
[8] H. J. Yoon, J. H. Kim, E. S. Choi, S. S. Yang, and K. W. Jung, "Fabrication of a novel micro time-of-flight mass spectrometer," *Sensors and Actuators*, vol. A97-8, pp. 441–447, 2002.
[9] R. G. Brewer, R. G. Devoe, and R. Kallenbach, "Planar ion microtraps," *Phys. Rev.*, vol. A46, pp. R6781–R6784, 1992.
[10] J. M. Wells, E. R. Badman, and R. G. Cooks, "A quadrupole ion trap with cylindrical geometry operated in the mass-selective instability mode," *Anal. Chem.*, vol. 70, pp. 438–444, 1998.
[11] E. R. Badman and R. G. Cooks, "A parallel miniature cylindrical ion trap array," *Anal. Chem.*, vol. 72, pp. 3291–3297, 2000.

[12] O. Kornienko, P. T. A. Reilly, W. B. Whitten, and J. M. Ramsey, "Micro ion trap mass spectrometry," *Rapid. Comm. in Mass Spect.*, vol. 13, pp. 50–53, 1999.

[13] M. J. Madsen, W. K. Hensinger, D. Stick, J. A. Ratschuk, and C. Monroe, "Planar ion trap geometry for microfabrication," *Appl. Phys. B-Lasers*, vol. O 78, pp. 639–651, 2004.

[14] O. Kornienko, P. T. A. Reilly, W. B. Whitten, and J. M. Ramsey, "Field-emission cold-cathode EI source for a microscale ion trap mass spectrometer," *Anal. Chem.*, vol. 72, pp. 559–562, 2000.

[15] L. Licklider, X. Q. Wang, A. Desai, Y. C. Tai, and T. D. Lee, "A micromachined chip-based electrospray source for mass spectrometry," *Anal. Chem.*, vol. 72, pp. 367–375, 2000.

[16] R. B. Darling, A. A. Scheidemann, K. N. Bhat, and T. C. Chen, "Micromachined Faraday cup array using deep reactive ion etching," *Sensors and Actuators*, vol. A95, pp. 84–93, 2002.

[17] W. Paul and H. Steinwedel, "Ein neues massenspektrometer ohne magnetfeld," *Z.f. Naturforschung*, vol. 8a, pp. 448–450, 1953.

[18] P. H. Dawson, *Quadrupole Mass Spectrometry and Its Applications*. Amsterdam, The Netherlands: Elsevier Scientific, 1976.

[19] J. H. Batey, "Quadrupole gas analyzers," *Vacuum*, vol. 37, pp. 659–668, 1987.

[20] O. J. Orient, A. Chutjian, and V. Garkanian, "Miniature, high-resolution, quadrupole mass-spectrometer array," *Rev. Sci. Instrum.*, vol. 68, pp. 1392–1397, 1997.

[21] S. Boumsellek and R. J. Ferran, "Miniature quadrupole arrays for residual and process gas analysis," *J. IEST*, vol. 42, pp. 27–31, 1999.

[22] D. Wiberg, N. V. Myung, B. Eyre, K. Shcheglov, O. Orient, E. Moore, and P. Munz, "LIGA fabricated two-dimensional quadrupole array and scroll pump for miniature gas chromatograph/mass spectrometer," *Proc. SPIE*, vol. 4878, pp. 8–13, 2003.

[23] R. R. A. Syms, T. J. Tate, M. A. Ahmad, and S. Taylor, "Fabrication of a microengineered quadrupole electrostatic lens," *Electron. Lett.*, vol. 32, pp. 2094–2095, 1996.

[24] R. R. A. Syms, T. J. Tate, M. M. Ahmad, and S. Taylor, "Design of a microengineered quadrupole electrostatic lens," *IEEE Trans. Electron Dev.*, vol. TED-45, pp. 2304–2311, 1998.

[25] S. Taylor, J. J. Tunstall, J. H. Leck, R. Tindall, P. Julian, J. Batey, R. R. A. Syms, T. J. Tate, and M. M. Ahmad, "Performance improvements for a miniature quadrupole with a micromachined mass filter," *Vacuum*, vol. 53, pp. 203–206, 1999.

[26] N. Sillon and R. Baptist, "Micromachined mass spectrometer," *Sensors and Actuators*, vol. B83, pp. 129–137, 2002.

[27] R. R. A. Syms, L. Michelutti, and M. M. Ahmad, "Two-dimensional microfabricated electrostatic einzel lens," *Sens. Actuators A, Phys.*, vol. A107, pp. 285–295, 2003.

[28] C. Marxer, P. Griss, and N. F. de Rooij, "A variable optical attenuator based on silicon micromechanics," *IEEE Photon. Tech. Lett.*, vol. 11, pp. 233–235, 1999.

[29] A. Benitez, J. Esteve, and J. Bausells, "Bulk silicon microelectromechanical devices fabricated from commercial bonded and etched-back silicon-on-insulator substrates," *Sens. Actuators A, Phys.*, vol. A50, pp. 99–103, 1995.

[30] E. H. Klaassen, K. Petersen, J. M. Noworolski, J. Logan, N. I. Maluf, J. Brown, C. Storment, W. McCulley, and T. A. Kovacs, "Silicon fusion bonding and deep reactive ion etching: A new technology for microstructures," *Sens. Actuators A, Phys.*, vol. A52, pp. 132–139, 1996.

[31] F. Laermer and A. Schilp, "Method of Anisotropically Etching Silicon," US 5 501 893, Mar. 26, 1996.

[32] N. Miki, X. Zhang, R. Khanna, A. A. Ayon, D. Ward, and S. M. Spearing, "Multi-stack silicon-direct wafer bonding for 3D MEMS manufacturing," *Sens. Actuators A, Phys.*, vol. A103, pp. 194–201, 2003.

[33] A. M. Hynes, H. Ashraf, J. K. Bhardwaj, J. Hopkins, I. Johnston, and J. N. Shepherd, "Recent advances in silicon etching for MEMS using the ASE™ process," *Sens. Actuators*, vol. 74, pp. 13–17, 1999.

[34] Y. Mita, A. Tixier, S. Oshima, M. Mita, J.-P. Gouy, and H. Fujita, "A silicon shadow mask with unlimited patterns and a mechanical alignment structure by al-delay masking process," *Trans. J. IEE*, vol. 120-E, pp. 357–362, 2000.

[35] K. T. Turner and S. M. Spearing, "Modeling of direct wafer bonding: Effect of wafer bow and etch patterns," *J. Appl. Phys.*, vol. 92, pp. 7658–7666, 2002.

[36] "NIST," Mass Spectral Library, Gaithersburg, MD.

Martin Geear received the B.Sc. degree in physics from the University of St Andrews, Scotland, in 1987 and the M.Sc. degree in laser and optoelectronic devices from Heriot-Watt University, Edinburgh, Scotland, in 1988.

He joined Nortel Networks (formerly STL) in 1988, where he gained broad experience in the development, manufacturing and product management of optoelectronic and MEMS technologies and devices. He joined Microsaic Systems in 2002, where he worked on the design and development of MEMS-based switches and a microengineered mass spectrometer. In 2004, he joined Dalsa Semiconducteur, based in Quebec, Canada, to work on production and development activities involving MEMS, CMOS, and CCD technologies.

Richard R. A. Syms (SM'02) was born in Norfolk, VA, in 1958. He received the B.A. degree in engineering science in 1979, and the D.Phil. degree (on volume holographic optical elements) in 1982, both from Worcester College, Oxford University, U.K.

He has been Head of the Optical and Semiconductor Devices Group in the Department of Electrical and Electronic Engineering, Imperial College London, U.K., since 1992 and Professor of Microsystems Technology since 1996. Prior to that, he was Reader in Electro-optics, Senior Lecturer and Senior Research Fellow at Imperial College, and prior to that, Atlas Research Fellow at Pembroke College, Oxford. He currently lectures on guided wave optics and MEMS at undergraduate and postgraduate level, at Imperial and elsewhere. He has published over 100 journal papers and two books on holography, guided-wave optics, and microengineering. Most recently, he has been developing electrical MEMS such as microconnectors, RF probes for magnetic resonance imaging, and miniature quadrupole mass spectrometers, optical MEMS devices such as alignment devices, variable optical attenuators and tunable lasers, and three-dimensional self-assembling microstructures. He was Co-Founder and has been Research Director of the MEMS spin-out company Microsaic Systems since 2001. He currently acts as an Associate Editor for the IEEE/ASME JOURNAL OF MICROELECTROMECHANICAL SYSTEMS.

Steven Wright was born in London, England, in 1970. He received the B.Sc. degree in chemistry in 1992 and the Ph.D. degree in physical chemistry in 1996, both from the University of Southampton, U.K.

Between 1995 and 2000, he undertook postdoctoral research at the Fritz Haber Institute, Berlin, Germany, Odense University, Denmark, the University of Essen, Germany, and the University of Liverpool, U.K. His research interests were in the field of chemical and photochemical reactions on single crystal surfaces. In 2000, he joined Applied Materials U.K., where he was involved with the development of ion implant systems. He joined Microsaic Systems, Ltd., in 2003, where he has been responsible for aspects of mass spectrometer design and development.

Andrew S. Holmes (M'02) received the B.A. degree in natural sciences from Cambridge University, U.K., in 1987 and the Ph.D. degree in electrical engineering from Imperial College London, U.K., in 1992.

He is currently a Reader in the Optical and Semiconductor Devices Group, Department of Electrical and Electronic Engineering, Imperial College London. His research interests are mainly in the areas of micropower generation and conversion, MEMS devices for microwave applications, and laser processing for MEMS manufacture. He was Co-Founder and has been Director of Engineering of the MEMS spin-out company Microsaic Systems since 2001.